Advanced Ceramics Progress: Vol. 10, No. 3, (Summer 2024) 8-14

Materials and Energy Research Center
MERC

Contents lists available at ACERP

Advanced Ceramics Progress

Journal Homepage: www.acerp.ir

Original Research Article

Effect of Sintering Parameters on the Densification of ZrB_2-SiC based Composite

Elnaz Irom [a], Mohammad Zakeri [b]*, Mansour Razavi [c]

[a] *PhD Candidate, Department of Ceramics, Materials and Energy Research Center, Karaj, Iran.*
[b] *Associate Professor, Department of Ceramics, Materials and Energy Research Center, Karaj, Iran.*
[c] *Professor, Department of Ceramics, Materials and Energy Research Center, Karaj, Iran.*
* Corresponding Author Email: m_zakeri@merc.ac.ir (M. Zakeri)

URL: https://www.acerp.ir/article_211776.html

ARTICLE INFO

Article History:
Received: 27 July 2024
Revised: 28 August 2024
Accepted: 01 September 2024

Keywords:
ZrB_2,
Densification,
Spark Plasma Sintering,
Porosity,
Density

ABSTRACT

In this study, ZrB_2-SiC ultra-high temperature ceramic composite was sintered using Spark Plasma Sintering (SPS) process with WC/HfB_2 modifiers at different sintering temperatures of 1850, 1900, 2000, and 2050˚C for 8 and 25 minutes. The densification behavior of the composite was also examined using punch displacement-time and temperature-time measurement graphs during SPS. Phase and microstructure evaluations were also done based on XRD, EDS, and FESEM methods. The effect of SPS parameters on the densification of ZrB_2-SiC-based composite was studied. In this case, there was no displacement until the pressure was applied due to the low sinterability of boride powders. A ZrB_2-SiC-based composite with a relative density of 90% was obtained at 2050˚C under 30 MPa for a 25-minute soaking time. The densification curve of this sample showed a typical "S" shape. The best water absorption and apparent porosity values obtained as 1.3 and 6.7%, respectively. The minimum and maximum punch displacement of the samples was 2.2 and 3.6 mm, respectively. Use of WC/HfB_2 modifiers led to the formation of byproducts of WB and HfB.

https://doi.org/10.30501/acp.2024.465234.1158

1. INTRODUCTION

High-temperature applications require structural ceramic composite parts that can withstand harsh environmental situations. Highly refractory materials, such as Ultra-High Temperature Ceramics (UHTCs) family, are some of the most encouraging candidates. They possess an acceptable functional, physical, and mechanical properties including considerable flexural strength, hardness, and fracture toughness, and very high melting point (>3000˚C). The new generation of thermal protection systems is designed to resist high heat flux, high temperature, and mechanical stress. Additionally, they should exhibit good heat shock resistance, oxidation resistance, and ablation resistance (Chakraborty et al., 2016; Jin et al., 2018).

Various consolidation processes have been employed to sinter the UHTCs, including pressure-less sintering (Wang et al., 2022), flash sintering (Foroughi et al., 2022), reactive hot pressing (Lu et al., 2016), hot pressing (Zou et al., 2013), Spark Plasma Sintering (SPS) (Thimmappa et al., 2019), and reactive SPS (Zhu et al., 2022). High-density UHTCs without sintering aids can be obtained by SPS with limited grain growth (Bellosi et al., 2006; Guo et al., 2008).

ZrB_2 is a key material with a lower density than other metal diboride ceramics. Pure ZrB_2 and modified ZrB_2 are considered potential alternatives for the last

Please cite this article as: Irom, E., Zakeri, M, & Razavi, M. (2024). Effect of Sintering Parameters on the Densification of ZrB2-SiC based Composite, *Advanced Ceramics Progress*, 10(3), 8-14. https://doi.org/10.30501/acp.2024.465234.1158

generations of heat-resistant structural materials. However, the ablation resistance of ZrB_2 is a challenging aspect of its performance in the field. SiC is regularly added to ZrB_2 to enhance its oxidation resistance (Carney et al., 2009; Fahrenholtz & Hilmas, 2012; Han et al., 2007, 2008).

Although many variations in UHTC compositions have been formulated to improve their high-temperature properties, few studies have focused on enhancing their densification along with other properties without additives. Based on previous works and our recent study, we produced a new ZrB_2-SiC composite, which is anticipated to exhibit better thermal properties and densification without adding sintering aids. The overall objective of this project was to examine the densification behavior of the HfB_2/WC modified ZrB_2-SiC bulk composite, produced through the SPS method. It is expected that using a higher sintering temperature and soaking time can improve the densification of this composite.

2. MATERIALS AND METHODS

Boride powders of ZrB_2 (99.9%, 3 µm), HfB_2 (99.9%, 5 µm), and carbide powders of SiC (99%, 70 nm), and WC (99%, 5 µm) were mixed in specific ratios (64.75 vol.% ZrB_2, 27.75 vol.% SiC, 5 vol.% WC, and 2.5 vol.% HfB_2) based on our previous works (Irom, 2023; Shalmani et al., 2021). Dispersion evolution was carried out in an ultrasonic bath for 30 min. After the mixing stage, the obtained suspension was homogenized in a heater-magnetic stirrer (Heidolph MR 3001, Germany) for 120 minutes. The composite powder mixture was then completely dried in an oven at 120℃ for 6 h. Consequently, the dried powder was sieved and poured into a graphite die with a diameter of 3 cm. The inner surface of the die was entirely covered with graphite foil. The sintering stage was performed by the SPS apparatus (SPS-20 T-10, Easy Fashion Metal Products Trade Co., China) in a vacuum atmosphere, with the chamber pressure monitored. The temperature of the graphite die was recorded with an optical pyrometer (Raytek, USA). Between room temperature and 1600 ℃, with a heating rate of 50℃/min, a primary uniaxial pressure of 10 MPa was used on the die. At the maximum SPS temperature (1850˚C-2050˚C), the applied pressure was gradually increased up to 30 MPa and maintained for 8 or 25 min. To treat the surface of the as-sintered sample, consequent grinding and polishing were operated on both sides. X-Ray Diffraction (PW3710, Philips, Netherlands) was utilized for crystalline phase characterization.

The microstructure of the samples was evaluated by Field Emission Scanning Electron Microscopy (FESEM) (TESCAN Mira 3-XMU, Czech Republic). Energy-Dispersive X-Ray Spectroscopy (EDS) analysis was then carried out for the semi-quantitative assessment of the composition of phases.

3. RESULTS AND DISCUSSION

Table 1 presents the relative density, water absorption, and porosity of sintered samples. As observed, the relative density increased with an increase in the sintering temperature. Consequently, both water absorption and porosity decreased with the progress in the relative density. Boride ceramics have low self-diffusion and are difficult to sinter (Venkateswaran et al., 2006). The SPS method significantly reduced the porosity and increased the relative density of this type of material due to the simultaneous application of mechanical pressure and heat during sintering. It should be noted that spark plasma discharges during SPS sintering clean the surfaces of the powders from CO_2 and H_2O that have already been absorbed, as well as the impurities that remain on the surface of the particles during powder synthesis, such as B_2O_3 or ZrO_2, and HfO_2. In the subsequent stages, the presence of clean and active surfaces increases the penetration of grain boundaries, which, together with spark plasma discharges, improves the transfer of matter and facilitates the condensation and growth of grains (R. Riedel and I.W. Chen, 2011). Higher temperature and soaking times provide more activation energy, removing the oxide impurities of the surface of the powder particles, resulting in the interaction of the composite powders. In this regard, active and clean surfaces accelerated grain boundary diffusion.

An experimental SPS parameter monitoring for ZSWH1 and ZSWH4 is represented in Figure 1, where not only the displacement was recorded but also the temperature, DC current, applied pressure, and vacuum pressure was monitored. As seen, the chamber pressure changed during the sintering process due to gas removal from the die system. The gas release at low temperature is caused by adsorbed water vapor and trapped air in the mixed powder while at high temperature, it originates from chemical reaction and gaseous byproducts. There is a peak at the beginning of the process which can be attributed to inappropriate mold preparation and powder pull-out in the chamber.

TABLE 1. Relative density water absorption porosity of samples

Sample	sintering Temperature (˚C)	Soaking time (min)	Relative Density (%)	Water absorption (%)	Apparent Porosity (%)
ZSWH1	1850	8	67.8	6.9	27.6
ZSWH2	1900	8	73.0	5.8	24.9
ZSWH3	2000	25	83.5	3.2	15.8
ZSWH4	2050	25	90.8	1.3	6.7

Once the displacement increased and densification started, the chamber pressure decreased. In both graphs, the vacuum fluctuated, and the chamber pressure in the beginning of the process around 1100℃ increased due to the formation of SiO and CO gases. The electrical current was gradually increased at the determined temperature and controlled until the sintering finished. Then, the DC current decreased with the rate of 0.2 KA/min.

The study of the displacement-time and temperature-time graph for sintering provides useful information. An increase in displacement indicates an increase in the powder shrinkage and provides a scale of condensation and sintering. The displacement values for ZSWH1(Fig1.a) and ZSWH4 (Fig.1b) were 2.2 mm and 3.6 mm, respectively. The densification curve of ZSWH4 shows a typical "S" shape.

To better study the graphs, they were divided into three zones based on displacement variations: Zone 1: there was no displacement, and the electrical power created joule heat, which warmed the die and the powder. Interestingly, no displacement occurred until the pressure was imposed mainly due to not using the sintering aids in the composition and covalent bonding, weak self-diffusion and consequently, low sinterability of the boride and carbide powders (Venkateswaran et al., 2006). There is an expansion zone in the displacement graphs as the process started, and the die temperature rose. As the temperature increased, the powder became smooth due to electrical pulses and heat. Zone 2: for ZSWH4, about 14 min after starting the process and when the temperature reached 1900˚C, the displacement improvement was observed upon increasing the pressure. As a result of plastic deformation and powder shrinkage, displacement was intensified, and the maximum displacement was obtained upon applying the pressure. Zone 3: in the ZSWH4 graph, where the temperature is 2050˚C and constant, the sintering process continued by diffusion and grain growth mechanism (Chaim, 2007; Marder et al., 2011). The low shrinkage in this zone can be attributed to the diffusion mechanism mainly because the diffusion is a slow and time-consuming process (Chaim, 2007; Marder et al., 2011). The SPS sensors cannot record the minor displacement variations; therefore, no displacement was observed in the third zone. Over time in this stage and grain growth, the porosity decreased while the relative density increased. Once the soaking time ended, the temperature was slowly reduced, and the pressure was gradually removed at 1600˚C. A comparison between the displacement and temperature graphs of the two samples reveals that after the end of the soaking time at the maximum temperature in the ZSWH1, the displacement did not remain constant. As a result, the densification process continued while the soaking time was not enough at this temperature. However, in the ZSWH4, prior to the end of the soaking time, the graph became stable, and the condensation continued with reduction in both the grain growth and porosity. It seems that the soaking time should be chosen in such a way that displacement becomes constant before the end of the time, and the displacement graph remains a little more fixed at the highest temperature. At this stage, the changes are insignificant, and the device cannot record them. The overlap of displacement and temperature graphs in the soaking region indicates the last step of sintering, i.e., grain growth and diffusion. In this area, i.e., at the maximum temperature and where the displacement is constant, the sample should be maintained for a few minutes until the sintering is complete.

Stabilization of displacement during cooling and non-overlapping of displacement graph with the temperature diagram in the soaking area is not desirable. Soaking time should be determined in such a way that displacement becomes constant within the soaking stage and grain growth occurs.

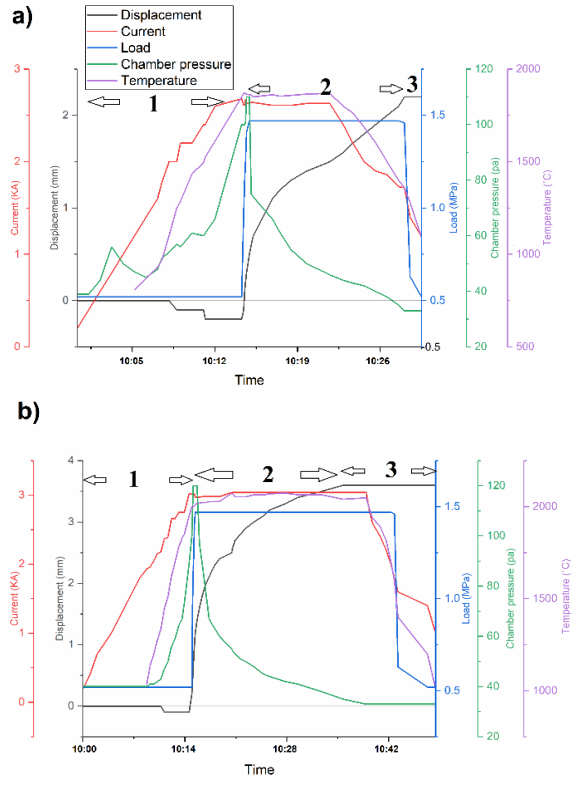

Figure 1. The displacement-time and temperature-time graph for sintering of a) ZSWH1 b) ZSWH4

Figure. 2 shows the XRD patterns of the as-sintered ZSWH3 sample. The composite consists of ZrB_2, SiC, and byproducts of WB and HfB. During the sintering process, WC and HfB_2 were converted into WB and HfB, respectively, as discussed below:

Under thermodynamical investigations, Monteverde et al. reported that WC interacted with superficial oxides of the ZrB_2 particles like molten SiO_2, as shown

in Reaction (1) at temperatures as low as 1130 ˚C and chamber pressure of about 100 Pa (Monteverde & Silvestroni, 2016).

$$WC_{(s)} + SiO_{2(l)} = W_{(s)} + SiO_{(g)} + CO_{(g)} \quad (1)$$

where WC and B_2O_3 oxide impurities originating from ZrB_2 and HfB_2 powders can react with each other based on Reaction (Irom, 2023):

$$3WC_{(s)} + B_2O_{3(l)} = 2WB_{(s)} + W_{(s)} + 3CO_{(g)} \quad (2)$$

On the other hand, Ding et al. indicated that at temperatures higher than 1700 ˚C, diffusion of B into W increased, hence formation of the WB phase (Ding et al., 2020). Free W element can also interact with HfB_2. It seems that penetration of B element from HfB_2 into W resulted in the creation of boron vacancies in HfB_{2-X}, coupled with the formation of HfB phase. Residual boron vacancies can lead to a qualified sintering process. More details about these interactions can be found in our previous work (Irom, 2023).

Beside WC/HfB_2 modifiers, SiC can act significantly followed by introduction of self-cleaning reactions between SiC and its surface oxide, i.e., SiO_2. In the same way, Reaction 3 occurs under standard conditions i.e., at the pressure of $p=10^5$ Pa and temperatures between 1527- 1677˚C. Reactions 3 and 4 occur at temperatures above 1677˚C, and surface SiO_2 impurity can be either eliminated (Shafagh et al., 2021).

$$SiC_{(s)} + SiO_{2(l)} = 3\,SiO_{(g)} + CO_{(g)} \quad (3)$$

$$SiC_{(s)} + SiO_{2(l)} = 3\,Si_{(l)} + 2\,CO_{(g)} \quad (4)$$

Based on Reaction 5, SiC can react with contaminations at temperatures above 1800˚C(Shafagh et al., 2021):

$$2.5SiC_{(s)}+B_2O_{3(l)}+ZrO_{2(s)}=ZrB_{2(s)}+2.5SiO_{(g)}+2.5CO_{(g)} \quad (5)$$

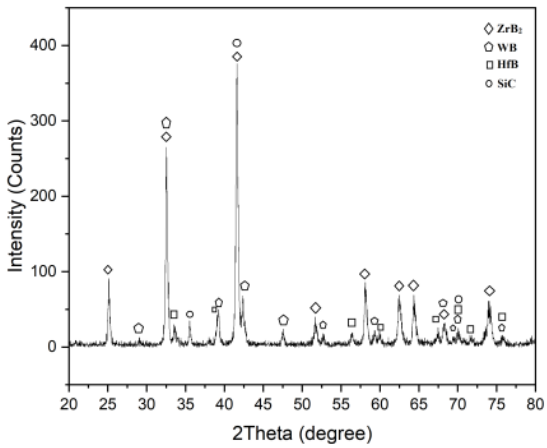

Figure 2. XRD patterns of the sample ZSWH3

Figure 3.a illustrates the secondary FESEM images of the polished surface of the ZSWH3. The sample shows a mosaic microstructure with a proper distribution of reinforcing phases within the ZrB_2 matrix. In Figure 3, the porosities are shown by arrows on the surface. Porosities are uniformly distributed through the surface.

Figure 3.b shows the backscattered FESEM image in a higher magnification.

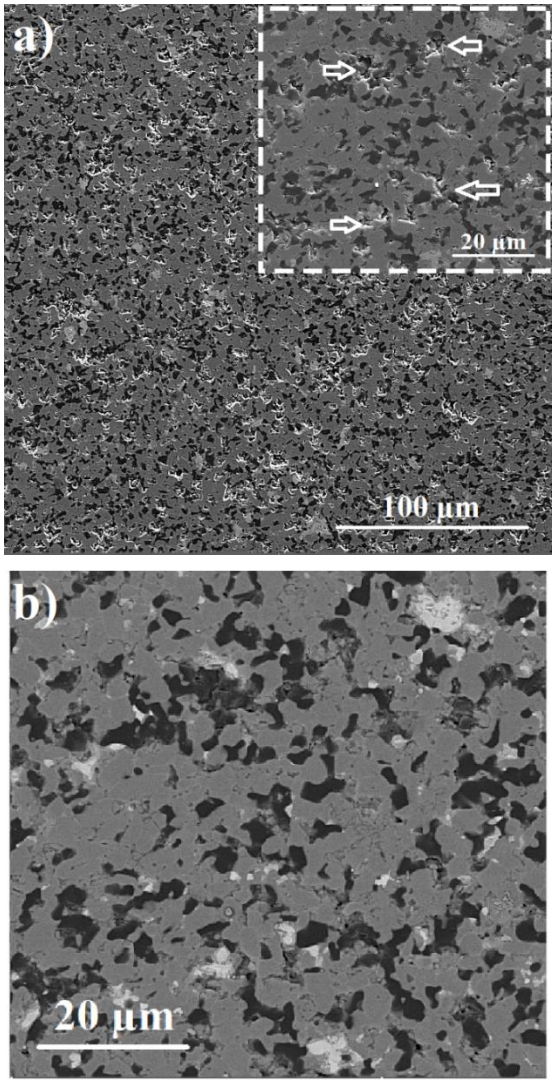

Figure 3. a) secondary, b) backscattered FESEM micrograph of the polished surface of the ZSWH3

Figure 4 represents the map analysis which was carried out to specify the phases. As indicated, the black phases are rich in Si which can be attributed to SiC. Light grey phase is rich in Hf and dark grey in Zr. To precisely determine the phases, point EDS analysis was done and according to different colors, five points were recognizable. As represented in Figure 5. (b), four various phases can be identified in the sample. Point A is attributed to SiC, point B to HfB, points C and D to ZrB_2, and point E to WB. The gray matrix is ZrB_2, and SiC, WB, and there is a slight weight percentage of W in the EDS of points of C and D.

Figure 5 confirms the presence of WB and HfB phases based on the XRD and EDS analyses. A

comparison of the points B and D reveals that the weight percentages of Zr and Hf in point C were 44.80 and 1.82% and in point D, they were 30.03 and 16.95%, respectively. It seems that Hf was diffused into the ZrB_2 grains during sintering, as already reported by Balak et al. (Balak, 2019). The W content of point D is also higher than that of point C which can be associated with the diffusion of W into the ZrB_2 grains. The free W element originating from Reactions 1 and 2 are also diffused into the matrix structure.

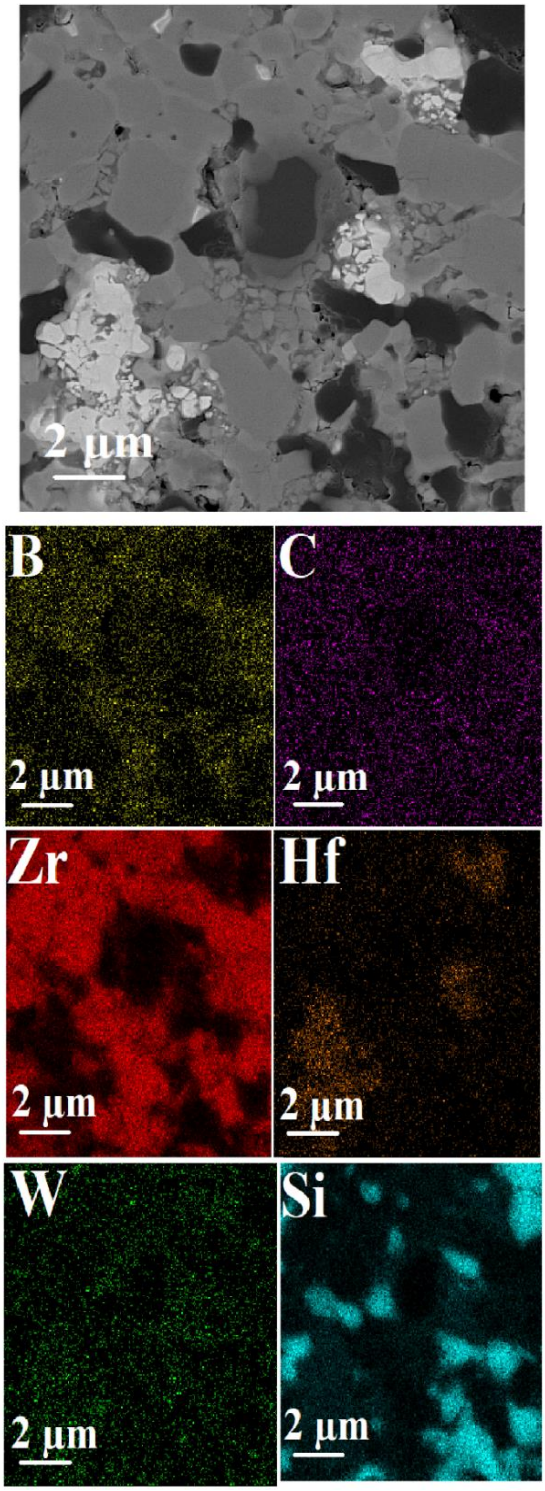

Figure 4. Map analysis of the ZSWH3

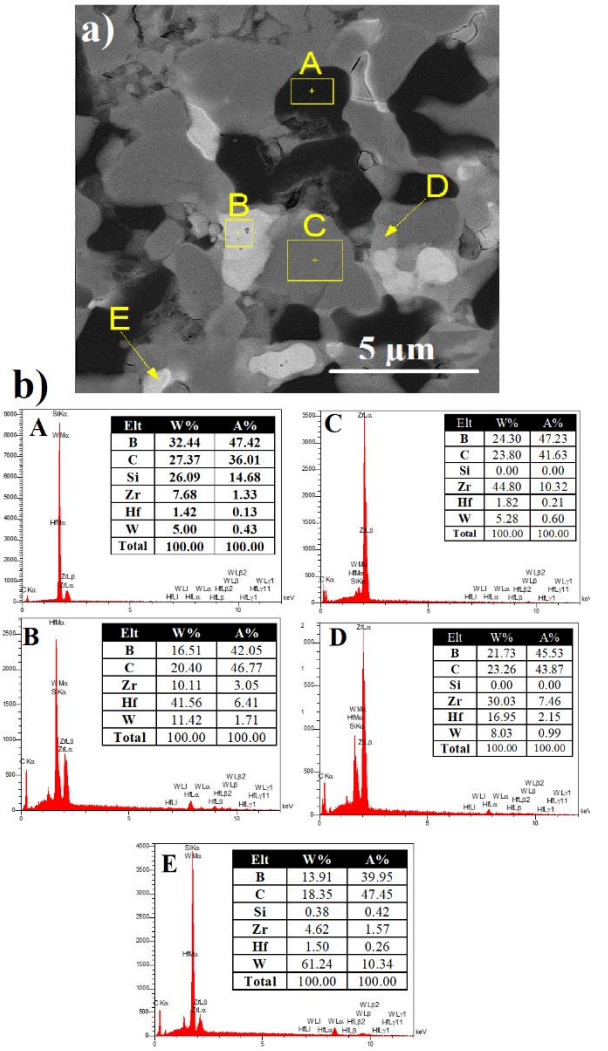

Figure 5. a) backscattered FESEM micrograph of the polished surface of the ZSWH3 B) EDS point analysis of the ZSWH3

4. CONCLUSION(S)

In this research, the ZrB_2-SiC composite was spark-plasma-sintered using WC/HfB_2 modifiers and Spark Plasma Sintering (SPS) method. The major findings are summarized in the following:

- New phases of WB and HfB were created during SPS. Followed by the diffusion of B into W, the WB phase was formed. It seems that penetration of B element from HfB_2 into W resulted in the creation of boron vacancies in HfB_{2-X}, coupled with the formation of HfB phase. WC and HfB_2 Modified the microstructure of ZrB_2-SiC by removing oxide contamination.

- Sintering the ZrB_2-SiC composite with boride or carbide modifiers needs a high temperature and soaking time. Increasing the sintering time and temperature led to higher final relative density.
- The densification behavior was examined based on the proposed densification mechanisms, and the densification was enhanced in three steps: plastic deformation, diffusion, and grain growth.
- When using four boride compounds, the last stage of sintering takes more time. In other words, diffusion and grain growth take more time to start and evolve.
- Interestingly, there was no displacement until the pressure was applied. It can be due to the low sinterability of boride powders and not using the sintering aids.
- The overlapping of the displacement and temperature diagram, which was actually indicative of the final stage of sintering, i.e., grain growth and diffusion, was necessary for sintering and completing condensation.

ACKNOWLEDGEMENT

This article has been extracted from the research project in the name of "Investigation of ablation and oxidation resistance of ZrB_2-SiC composite doped with WC and HfB_2" which was supported by Materials and Energy Research Center.

REFERENCES

1. Balak, Z. (2019). Shrinkage, hardness and fracture toughness of ternary ZrB_2–SiC-HfB_2 composite with different amount of HfB_2. *Materials Chemistry and Physics*, *235*, 121706. https://doi.org/10.1016/j.matchemphys.2019.05.094
2. Bellosi, A., Monteverde, F., & Sciti, D. (2006). Fast densification of ultra-high-temperature ceramics by spark plasma sintering. *International Journal of Applied Ceramic Technology*, *3*(1), 32–40. https://doi.org/10.1111/j.1744-7402.2006.02060.x
3. Carney, C. M., Mogilvesky, P., & Parthasarathy, T. A. (2009). Oxidation behavior of zirconium diboride silicon carbide produced by the spark plasma sintering method. *Journal of the American Ceramic Society*, *92*(9), 2046–2052. https://doi.org/10.1111/j.1551-2916.2009.03134.x
4. Chaim, R. (2007). Densification mechanisms in spark plasma sintering of nanocrystalline ceramics. *Materials Science and Engineering: A*, *443*(1–2), 25–32. https://doi.org/10.1016/j.msea.2006.07.092
5. Chakraborty, S., Das, P. K., & Ghosh, D. (2016). Spark Plasma Sintering and Structural Properties of ZrB2 Based Ceramics: A Review. *Reviews on Advanced Materials Science*, *44*(2). http://www.ipme.ru/e-journals/RAMS/no_24416/06_24416_das.pdf
6. Ding, H.-J., Wang, X.-G., Xia, J.-F., Bao, W.-C., Zhang, G.-J., Zhang, C., & Jiang, D.-Y. (2020). Effect of solid solution and boron vacancy on the microstructural evolution and high temperature strength of W-doped ZrB_2 ceramics. *Journal of Alloys and Compounds*, *827*, 154293. https://doi.org/10.1016/j.jallcom.2020.154293
7. Fahrenholtz, W. G., & Hilmas, G. E. (2012). Oxidation of ultra-high temperature transition metal diboride ceramics. *International Materials Reviews*, *57*(1), 61–72. https://doi.org/10.1179/1743280411Y.0000000012
8. Foroughi, P., Durygin, A., Sun, S., & Cheng, Z. (2022). Flash sintering of tantalum-hafnium diboride solid solution powder. *Journal of Materials Research*, *37*(13), 2150–2156. https://doi.org/10.1557/s43578-022-00492-7
9. Guo, S., Nishimura, T., Kagawa, Y., & Yang, J. (2008). Spark plasma sintering of zirconium diborides. *Journal of the American Ceramic Society*, *91*(9), 2848–2855. https://doi.org/10.1111/j.1551-2916.2008.02587.x
10. Han, J., Hu, P., Zhang, X., & Meng, S. (2007). Oxidation behavior of zirconium diboride–silicon carbide at 1800° C. *Scripta Materialia*, *57*(9), 825–828. https://doi.org/10.1016/j.scriptamat.2007.07.009
11. Han, J., Hu, P., Zhang, X., Meng, S., & Han, W. (2008). Oxidation-resistant ZrB_2-SiC composites at 2200 °C. *Composites Science and Technology*, *68*(3–4), 799–806. https://doi.org/10.1016/j.compscitech.2007.08.017
12. Irom, E. (2023). *Investigation of thermal and mechanical resistance of ZrB_2-SiC composite doped with WC and HfB_2*. Materials and Energy Research Center [In Persian]. https://elmnet.ir/doc/10940655-79158
13. Jin, X., Fan, X., Lu, C., & Wang, T. (2018). Advances in oxidation and ablation resistance of high and ultra-high temperature ceramics modified or coated carbon/carbon composites. *Journal of the European Ceramic Society*, *38*(1), 1–28. https://doi.org/10.1016/J.JEURCERAMSOC.2017.08.013
14. Lu, Y., Zhang, G.-J., Liu, J.-X., Liu, H.-L., Wang, X.-G., & Xu, F.-F. (2016). Reactive hot-pressing of ZrB_2-ZrC-SiC ceramics via direct addition of SiC. *Ceramics International*, *42*(15), 16474–16479. https://doi.org/10.1016/j.ceramint.2016.06.167
15. Marder, R., Chaim, R., Chevallier, G., & Estournès, C. (2011). Densification and polymorphic transition of multiphase Y_2O_3 nanoparticles during spark plasma sintering. *Materials Science and Engineering: A*, *528*(24), 7200–7206. https://doi.org/10.1016/j.msea.2011.06.044
16. Monteverde, F., & Silvestroni, L. (2016). Combined effects of WC and SiC on densification and thermo-mechanical stability of ZrB2 ceramics. *Materials and Design*, *109*, 396–407. https://doi.org/10.1016/j.matdes.2016.06.114
17. Riedel, R., & Chen, I. W. (Eds.). (2011). *Ceramics Science and Technology, Synthesis and processing, vol. 3*. John Wiley & Sons. https://books.google.com/books?hl=en&lr=&id=eSrq6LRZ2rgC&oi=fnd&pg=PR15&dq=17.%09R.+Riedel+and+I.W.+Chen.+(2011).+Ceramics+Science+and+Technology,+Synthesis+and+processing,+vol.+3.+John+Wiley+%26+Sons.&ots=7ePna0iZtv&sig=mDCnkb-Twj6Q6tWEZh-Xo-Mx2VI
18. Shafagh, S. H., Jafargholinejad, S., & Javadian, S. (2021). Beneficial effect of low BN additive on densification and mechanical properties of hot-pressed ZrB_2–SiC composites. *Synthesis and Sintering*, *1*(2), 69–75. https://doi.org/10.53063/synsint.2021.1224
19. Shalmani, S. A. A., Sobhani, M., Mirzaee, O., & Zakeri, M. (2021). Ablation resistance of graphite coated by spark plasma sintered ZrB_2–SiC based composites. *Boletín de La Sociedad Española de Cerámica y Vidrio*. https://doi.org/10.1016/j.bsecv.2021.05.004
20. Thimmappa, S. K., Golla, B. R., Prasad, V. V. B., Majumdar, B., & Basu, B. (2019). Phase stability, hardness and oxidation behaviour of spark plasma sintered ZrB_2-SiC-Si_3N_4 composites. *Ceramics International*, *45*(7), 9061–9073. https://doi.org/10.1016/j.ceramint.2019.01.243
21. Venkateswaran, T., Basu, B., Raju, G. B., & Kim, D. Y. (2006). Densification and properties of transition metal borides-based cermets via spark plasma sintering. *Journal of the European Ceramic Society*, *26*(13), 2431–2440. https://doi.org/10.1016/J.JEURCERAMSOC.2005.05.011

22. Wang, S., Yang, Y., Cui, J., Liu, X., Zhang, S., & Jia, Q. (2022). Preparation and properties of porous ZrB_2 ceramics via combining in-situ boro/carbothermal reduction and partial sintering approach. *Ceramics International*, *48*(18), 27051–27063. https://doi.org/10.1016/j.ceramint.2022.06.017

23. Zhu, M., Zhang, L., Li, N., Cheng, D., Zhang, J., Yu, S., Bai, H., & Ma, H. (2022). Microstructures and mechanical properties of reactive spark plasma-sintered ZrB_2–SiC–$MoSi_2$ composites. *Ceramics International*, *48*(19), 27401–27408. https://doi.org/10.1016/j.ceramint.2022.05.378

24. Zou, J., Zhang, G.-J., Zhang, H., Huang, Z.-R., Vleugels, J., & Van der Biest, O. (2013). Improving high temperature properties of hot pressed ZrB_2–20vol%SiC ceramic using high purity powders. *Ceramics International*, *39*(1), 871–876. https://doi.org/10.1016/j.ceramint.2012.06.018